Translational Oncology
www.transonc.com

Volume 7 Number 4 August 2014 pp. 484–492 484

Characterization of the Inflammatory Microenvironment and Identification of Potential Therapeutic Targets in Wilms Tumors[1, 2]

Paramahamsa Maturu*,¶, Willem W. Overwijk†, John Hicks‡, Suhendan Ekmekcioglu†, Elizabeth A. Grimm† and Vicki Huff*,§

*Department of Genetics, The University of Texas MD Anderson Cancer Center, Houston, TX 77030, USA; †Department of Melanoma Medical Oncology, The University of Texas MD Anderson Cancer Center, Houston, TX, USA; ‡Department of Pathology, Texas Children's Hospital, Houston, TX, USA; §Graduate Program in Genes and Development and Graduate Program in Human Molecular Genetics, The University of Texas Graduate School of Biomedical Sciences, Houston, TX 77030, USA; ¶Department of Pediatrics, Section of Neonatology, Texas Children's Hospital, Baylor College of Medicine, Houston, TX 77030, USA

Abstract

The role of inflammation in cancer has been reported in various adult malignant neoplasms. By contrast, its role in pediatric tumors has not been as well studied. In this study, we have identified and characterized the infiltration of various inflammatory immune cells as well as inflammatory markers in Wilms tumor (WT), the most common renal malignancy in children. Formalin-fixed paraffin-embedded blocks from tumors and autologous normal kidneys were immunostained for inflammatory immune cells (T cells, B cells, macrophages, neutrophils, and mast cells) and inflammatory markers such as cyclooxygenase-2 (COX-2), hypoxia-inducible factor 1α, phosphorylated STAT3, phosphorylated extracellular signal–related kinases 1 and 2, inducible nitric oxide synthase, nitrotyrosine, and vascular endothelial growth factor expression. Overall, we found that there was predominant infiltration of tumor-associated macrophages in the tumor stroma where COX-2 was robustly expressed. The other tumor-associated inflammatory markers were also mostly localized to tumor stroma. Hence, we speculate that COX-2–mediated inflammatory microenvironment may be important in WT growth and potential therapies targeting this pathway may be beneficial and should be tested in clinical settings for the treatment of WTs in children.

Translational Oncology (2014) 7, 484–492

Introduction

The importance of inflammation in tumor development is well known, and it is apparent that an inflammatory microenvironment is a key component of many tumors, even when a clinical association with inflammation is not yet demonstrated [1–3]. During the past decade, studies using cell-specific knockout animals have elucidated mechanisms by which inflammation leads to cancer [4]. Inflammation is initiated by the recruitment of a wide range of inflammatory immune cells, which induce tumor cells to produce inflammatory mediators such as chemokines and cytokines, reactive oxygen and nitrogen species, and various other bioactive molecules, which work in an autocrine and/or paracrine manner [2]. In some instances, genetic as well as epigenetic modifications can also establish an

Address all correspondence to: Dr. Paramahamsa Maturu, Ph.D, Department of Pediatrics, Section of Neonatology, Texas Children's Hospital, Baylor College of Medicine, 1102 Bates Avenue, MC: FC520, Houston, TX 77030, USA. E-mail: maturu@bcm.edu

[1] This article refers to supplementary materials, which are designated by Tables W1 to W3 and Figure W1 and are available online at www.transonc.com.

[2] This work was supported by US National Institutes of Health grants CA34936 and DK069599 and by State of Texas Cancer Prevention Research Institute of Texas (CPRIT) grants RP110324 and RP100329 (V.H.). This work was partially supported by grants from the MD Anderson Cancer Center Specialized Programs of Research Excellence (SPORE) in Melanoma P50 CA093459 (E.A.G. and S.E.), by the MD Anderson Cancer Center Support grant P30 CA016672, and by the Dr Miriam and Sheldon G. Adelson Medical Research Foundation (E.A.G. and S.E.). The authors declare that there are no conflicts of interest.
Received 11 March 2014; Revised 10 May 2014; Accepted 21 May 2014

1936-5233/14
http://dx.doi.org/10.1016/j.tranon.2014.05.008

Table 1. Number of Sections that Stained Positive for Each Immune Cell Type and Inflammatory Marker Analyzed

CD3	CD20	TAM	TIN	MC	COX-2	HIF-1	p-Stat3	p-ERK1/2	iNOS	NT	VEGF
10/14	7/14	13/14	12/14	12/14	12/12	7/7	10/13	10/14	11/13	13/13	13/13

inflammatory microenvironment to promote tumor progression [1]. Thus, there exists a delicate balance between antitumor immunity and tumor-promoting immune activity within the tumor microenvironment, involving tumor cells, stroma (including fibroblasts and endothelial cells), and innate and adaptive immune cells.

The role of an inflammatory microenvironment in tumor development has been investigated primarily in adult-onset cancers, often those for which inflammation is a known risk factor. Little is known about the role of an inflammatory microenvironment in the development and growth of childhood tumors. Wilms tumor (WT) is a childhood cancer of the kidney that is thought to be largely a result of genetic alterations, variably including mutations in the *WT1*, *CTNNB1*, and/or *WTX1* genes. Vascular endothelial growth factor (VEGF) and hypoxia-inducible factor 1 (HIF-1), two proteins that are upregulated in the inflammatory environment and recruit inflammatory immune cells, have been observed in WT [5]. In a comparative analysis with adult tumors, infiltration of macrophages [6] was reported along with ubiquitous expression of cyclooxygenase-2 (COX-2) in a small set of pediatric tumors (including five WTs), and this infiltration and expression were independent of the type of neoplasm [7,8]. However, these studies were restricted to only one inflammatory marker, and none of the studies provided a comprehensive view of the inflammatory microenvironment in pediatric tumors or correlated the presence of these markers with inflammation in WT.

To learn more about the role of the inflammatory microenvironment in the development of WT, we analyzed tumors for various inflammatory markers and inflammatory immune cells by immunohistochemical (IHC) staining. Overall, we found that WT exhibited infiltration of inflammatory immune cells and overexpression of several inflammatory transcription factors and other inflammatory markers compared with normal kidneys. Our data suggest that a COX-2–mediated inflammatory microenvironment may be important in WT tumorigenesis and that investigating the potential utility of therapeutic targeting of this environment is warranted.

Materials and Methods

Tissue Samples

Pretreatment tumor tissues and autologous normal kidney specimens were obtained from 16 WT patients aged 7 to 66 months at the time of diagnosis. Informed consent was obtained from each patient's parent or guardian. Studies were approved by the Institutional Review Board and in accordance with an assurance filed with and approved by the US Department of Health and Human Services. Eight of the patients were males and eight were females, and one patient had bilateral disease. Of these 16 patients, 4 were at stage IV, 4 were at stage III, 3 were at stage II, and 5 were at stage I of WT disease. Tissues were fixed in formalin and embedded in paraffin (FFPE) in preparation for analysis.

Mouse Tumor Tissues

A mouse model for the human WT has been generated in our laboratory [9] by *Wt1* gene ablation and *insulin-like growth factor 2* (*IGF2*) upregulation by conditional knockout strategy (*Wt1*$^{-/fl}$*H19*$^{+/-m}$*Cre-ER*^{TM} *or Wt1-IGF2* mice). These mice developed tumors at the age of 3 months on an average. The tumors and normal kidneys from its littermate controls were collected at the similar age and processed as mentioned earlier for histology and IHC analysis.

Histology and IHC of Immune Cell Markers

FFPE specimens were cut in 5-μm sections, which were stained with hematoxylin and eosin. For IHC analysis, FFPE sections were deparaffinized in xylene, rehydrated sequentially in ethanol (100%, 90%, and 70%), and placed into a 1% phosphate-buffered saline solution (PBS; pH 7.4). Tissues were analyzed for infiltration by T cells, B cells, macrophages, neutrophils, and mast cells (MCs). Inflammatory markers analyzed were COX-2, HIF-1, phosphorylated extracellular signal–related kinases 1 and 2 (p-ERK1/2), phosphorylated STAT3 (p-Stat3), inducible nitric oxide synthase (iNOS), nitrotyrosine (NT), and VEGF. Simultaneously, to prove the similar expression and infiltration pattern in the mouse model of WT, mouse tumor tissues and control kidneys were immunostained for inflammatory marker COX-2 and predominant inflammatory immune cells, macrophages (F4/80). Details of antibody staining and epitope retrieval are summarized in Table W1.

Tissues known to contain the antigen of interest were identified and used as positive controls to optimize IHC staining by testing antigen retrieval methods and times and by titrating antibody dilutions. A positive control tissue slide was included in each batch of immunostaining. Negative controls were tissue sections not treated with the primary antibody. The numbers of sections assessed for each tumor for different immune cells and inflammatory protein markers are indicated in Table 1. Because of limitations in the amount of tumor tissue available, IHC data could not be obtained for all tumors.

MC Staining

MC infiltration in tumors and normal kidneys was assessed by quantification of chloroacetate esterase (Cat. No. 91C kit; Sigma Chemical Co, St Louis, U.S.A.). Briefly, immediately before fixation, 1 ml of sodium nitrite solution was added to 1 ml of Fast Red Violet LB base solution in a test tube and mixed gently by inversion and allowed to stand for 2 minutes. This solution was added to 40 ml of prewarmed (at 37°C) deionized water and then to 5 ml of Trizmal 6.3 buffer concentrate; afterwards, 1 ml of naphthol AS-D chloroacetate solution was added to obtain a red colored solution that was transferred into a Coplin jar. Slides were fixed in citrate acetone formaldehyde solution at room temperature (23-26°C) for 30 seconds. Slides were rinsed in running water for 45 to 60 seconds and incubated in previously prepared red colored solution for 15 minutes in Coplin jar at 37°C protected from light. Slides were rinsed with deionized water for 2 minutes and counterstained by Mayer's hematoxylin (Fisher Scientific, Fair Lawn, NJ) and mounted by aqueous mounting media. After drying, slides were evaluated microscopically.

Double Immunofluorescence Analysis

To examine the co-distribution of inflammatory marker COX-2 and tumor-associated macrophage (TAM) infiltration in the tumor stroma, a double immunofluorescence staining was carried out.

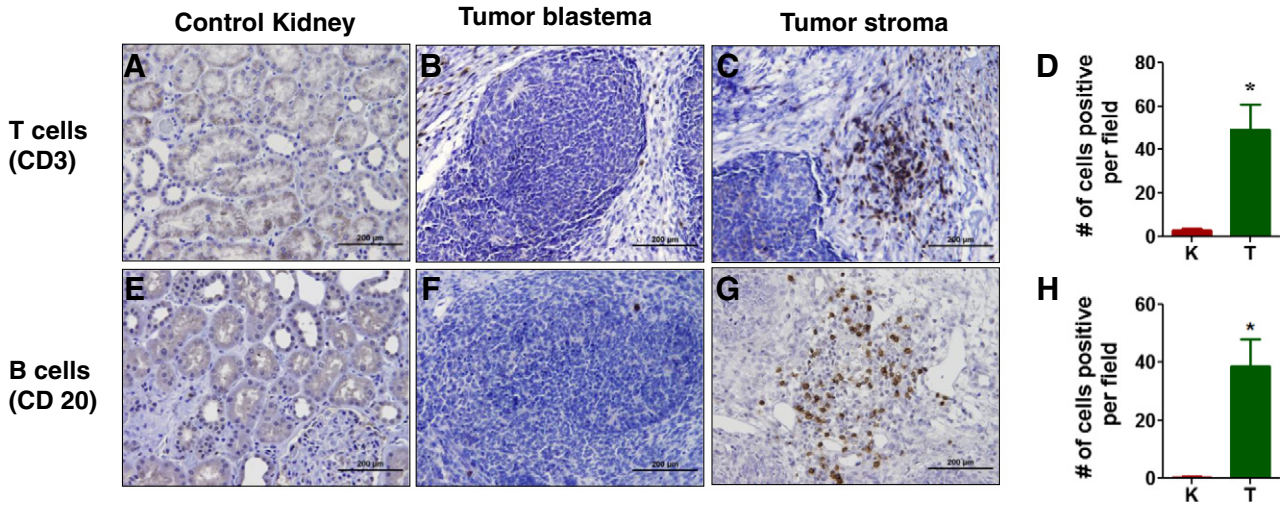

Figure 1. Localization of adaptive immune cell infiltration primarily in the stroma of WTs. (A–C) Representative CD3+ T cell infiltration on IHC analysis of (A) normal kidney, (B) tumor blastema, and (C) and tumor stroma. (D) Quantification of average number of CD3+ cells per field in normal kidneys (K) and tumors (T). (E–G) Representative CD20+ B cell infiltration on IHC analysis of (E) normal kidney, (F) tumor blastema, and (G) tumor stroma. (H) Quantification of average number of CD20+ cells per field in kidneys and tumors. *$P \leq .05$.

Briefly, after deparaffinization, the epitope retrieval was performed by heating for 45 minutes in 1 mM Tris EDTA, pH 9.0 buffer in a water bath at 95 to 100°C. The sections were left at room temperature in the buffer for 1 hour to cool down followed by washing three times with 1× PBS for 5 minutes each and were incubated with 1% BSA to block nonspecific protein binding. Sections were incubated overnight with a mixture of two primary antibodies [for macrophages, monoclonal mouse anti-human CD68 at 1:50 dilution (Dako, Glostrup, Denmark; Cat. No. M0814); for COX-2, polyclonal goat anti-human COX-2, 1:100 dilution (Santa Cruz Biotechnology, Dallas, Texas; SC-1747)] in 1% BSA in a humidified chamber at 4°C. After washing with 1× PBS three times, sections were incubated with a mixture of Alexa Fluor goat anti-mouse 555 and Alexa Fluor donkey anti-goat 488 in 1% BSA for 1 hour at room temperature in the dark. The mixture of secondary antibody solution was decanted and washed three times with PBS for 5 minutes each in the dark. Slides were mounted with coverslip with prolong Gold anti-fade mounting media with 4′,6-diamidino-2-phenylindole (DAPI). Finally, coverslips were sealed with nail polish to prevent drying and stored in the dark at 4°C. Double-label immunofluorescence was analyzed by means of an Olympus BX60 microscope equipped with different excitation and emission filters at ×200 magnification.

Quantification of Immune Cells and Inflammatory Markers

Ten to 15 representative high-power field images at ×200 magnification were collected for each tumor using an Olympus BX60 microscope. Each immune cell type was quantified in these images using NIS Elements software. Similarly, expression of the inflammatory markers was quantified by the sum density measurements of their expression using NIS Elements software.

Statistical Analysis

Two-tailed Mann-Whitney analysis with a 95% confidence interval was employed to establish statistical significance of differences between tumors and control kidneys. A value of $P < .05$ was considered statistically significant.

Results

Increased Inflammatory Immune Cell Infiltration in WTs

CD3+ T cells and CD20+ B cells. Significant CD3+ T cell infiltration was observed in 10 of 14 tumors relative to normal kidney (representative images shown in Figure 1, *A–C*). This infiltration was observed primarily in the stromal component of the tumor (Figure 1*C*) rather than in the epithelial and blastemal components (Figure 1*B*). Overall, tumors had 50 times more CD3+ T cells than normal kidneys (Figure 1*D*). Similarly, B lymphocytes (CD20+) were also present almost exclusively in the stroma of tumors (Figure 1, *E–G*). Unlike T cell infiltration, however, which was observed in all tumors, only 7 of 14 tumors analyzed showed substantial B cell infiltration. In the other seven tumors, very few B cells were detected. Overall, however, the average number of B cells infiltrated into tumors was significantly higher than in control kidneys (Figure 1*H*).

CD68+ TAMs. Infiltration by TAMs was observed in 13 of 14 tumors analyzed (Figure 2, *A–C*). TAM infiltration was observed primarily in stromal areas of tumors (Figure 2*C*), although some infiltrating TAMs were found in tumor blastemal and epithelial components (Figure 2*B*). Overall, there were significantly higher numbers of TAMs in tumors than in control kidneys (Figure 2*D*). The infiltration pattern and density of TAMs were uniform within the tumor in all the tumor cases analyzed.

Myeloperoxidase-positive neutrophils. The infiltration pattern of myeloperoxidase (MPO)–positive tumor-infiltrating neutrophils (TINs) was similar to that of TAMs. In 12 of 14 tumors analyzed, TIN infiltration was distributed in all regions of the tumor, but predominantly in the tumor stroma, with very few TINs in normal kidney sections (Figure 2, *E–G*). There were ~25 times more TINs in tumors than in normal kidneys (Figure 2*H*).

Mast cells. MCs were found principally in the stroma and in very small regions of the blastema; very few were found in normal tissues (Figure 2, *I–K*). Although 12 of the 14 tumors evaluated showed MC infiltration, the absolute numbers of MCs were much less than the other innate immune cells. The average number of MCs was significantly

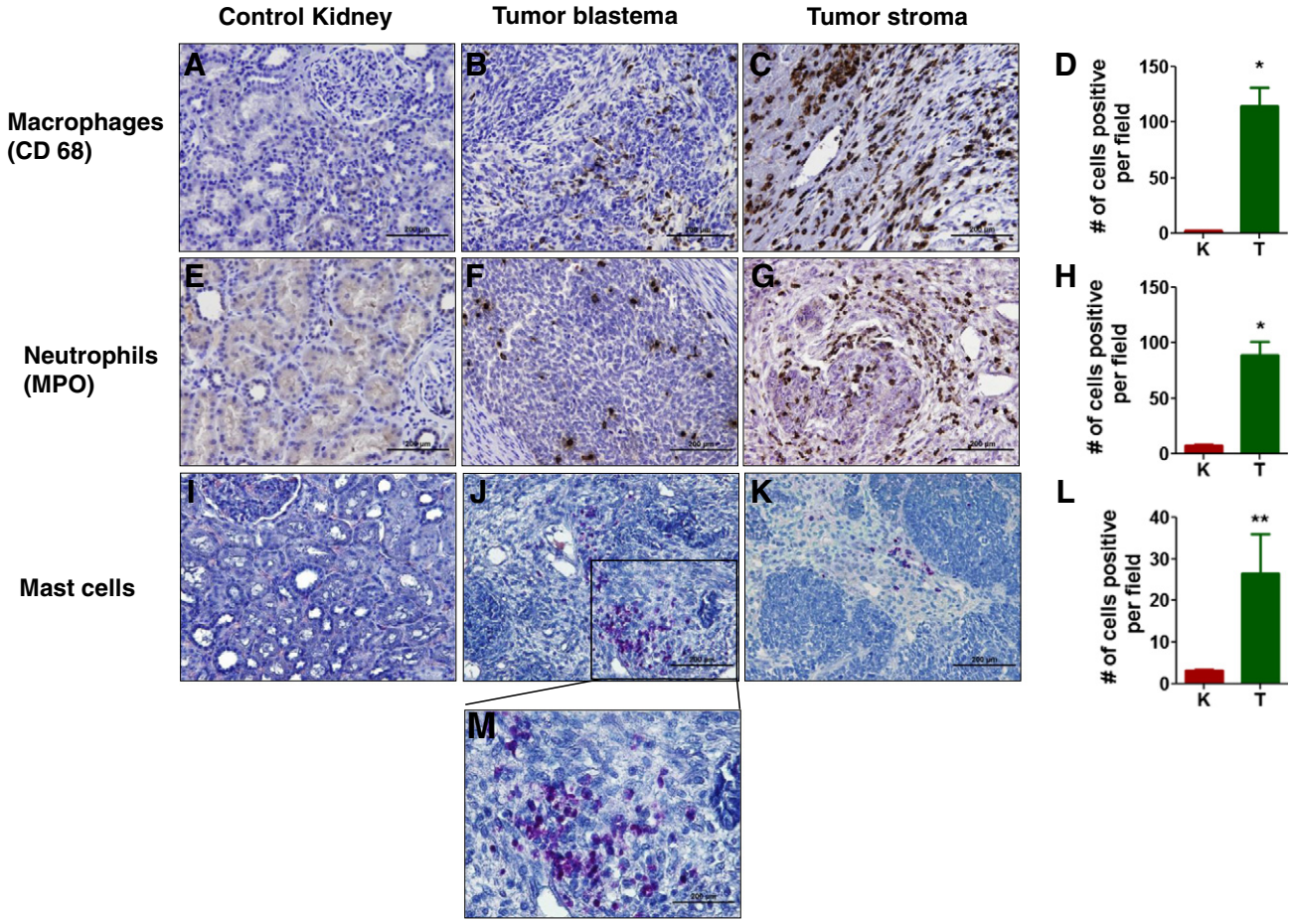

Figure 2. Infiltration of innate immune cells into WTs. (A–C) Representative infiltration by tumor-associated CD68+ macrophages (TAMs) on IHC staining of (A) normal kidney, (B) tumor blastema, and (C) tumor stroma. (D) Quantification of average number of TAMs per field in normal kidneys (K) and tumors (T). (E–G) Representative images of TINs (MPO-positive) on IHC analysis of (E) normal kidney, (F) tumor blastema, and (G) tumor stroma. (H) Quantification of average number of TINs per field in normal kidneys and tumors. (I–K) Representative MC staining in (I) normal kidneys, (J) tumor blastema, and (K) tumor stroma. (L) Quantification of average number of MCs per field. (M) Higher magnification images of MC infiltration in blastema and stroma. $*P \leq .05$, $**P \leq .01$.

higher in the tumors than in the normal kidney tissues (Figure 2*L*). Higher magnification of MCs infiltrating the blastema and stroma is shown in Figure 2*M*.

Therefore, both adaptive and innate immune cells were present in tumors at a much higher frequency than in normal kidneys. Comparison of the various infiltrative inflammatory immune cells in tumors showed that the degree of TAM infiltration was significantly higher than the degree of infiltration by the other cells (Figure 3). Infiltration pattern of various inflammatory immune cells in different parts of the tumor was summarized in Table W2.

Overexpression of Inflammatory Protein Markers in WTs

Cyclooxygenase-2. Positive immunoreactivity for the COX-2 protein was observed in all tumors assessed relative to normal kidney (Figure 4, *A–C*). In most tumors, weak to moderate cytoplasmic COX-2 expression was observed in blastemal and epithelial components and very intense nuclear staining was observed in the tumor stroma (Figure 4*C*), although some of the tumors also showed intense cytoplasmic expression in blastemal and epithelial cells (not shown). Normal kidney samples showed weak to moderate staining in the cytoplasm of some tubular epithelial cells (Figure 4*A*) and very weak or no staining in renal interstitial cells or glomeruli. The sum density of COX-2 expression was significantly higher (about five times) in tumors than in normal kidneys (Figure 4*D*).

Hypoxia-inducible factor 1. Although very little HIF-1 expression was noted in normal kidney slides (Figure 4*E*), seven of the seven tumors evaluated had cytoplasmic granular staining and membranous expression in blastemal and epithelial cells (Figure 4*F*), with very prominent nuclear localization of HIF-1 protein expression in the tumor stroma (Figure 4*G*). The density of HIF-1 expression in tumors was significantly higher than that in control kidneys (Figure 4*H*). The stromal expression of HIF-1 was similar to the COX-2 expression pattern (Figure 4, *C* and *G*).

Phosphorylated Extracellular Signal–Related Kinases 1 and 2. Cytoplasmic expression of p-ERK1/2 in normal kidney was negligible (Figure 4*I*). In contrast, prominent nuclear p-ERK1/2 staining was observed in 10 of the 14 tumors analyzed. Although some expression in blastemal cells (Figure 4*J*) was observed, p-ERK1/2 expression was primarily localized to tumor stroma (Figure 4, *K* and *L*). No p-ERK1/2 expression was observed in the epithelial component of tumors (not shown). Expression of p-ERK1/2 was significantly higher in tumors than in control kidneys (Figure 4*L*). The stromal expression pattern of p-ERK1/2 was similar to those of COX-2, HIF-1, and VEGF.

Phosphorylated STAT3. p-Stat3 expression was predominantly confined to the nucleus, with almost undetectable cytoplasmic staining

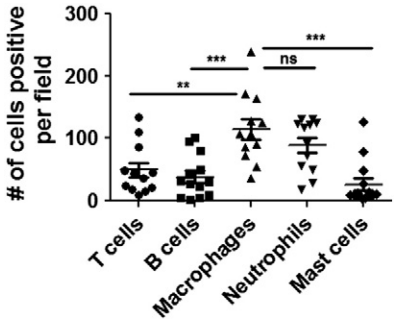

Figure 3. Proportions of various inflammatory immune cells' infiltration into WTs. Infiltration was quantified, and each different immune cell type was designated with a distinct symbol. Infiltration of TAMs was significantly greater than that of any other immune cell type. $^{**}P \leq .01$, $^{***}P \leq .001$; ns, not significant.

in 10 of 13 the WT evaluated (Figure 4, *M*–*O*). No p-Stat3 expression was detected in three of the tumors. Almost all p-Stat3 expression was in blastema (Figure 4*N*) or stroma (Figure 4*O*). Very little or no p-Stat3 expression was observed in the epithelial component of the tumors (not shown). p-Stat3 expression was significantly higher in tumors than in normal kidney (Figure 4*P*).

Inducible nitric oxide synthase. No significant immunoreactivity for iNOS was detected in the control kidney sections (Figure 5*A*). In contrast, very diffuse cytoplasmic staining was observed in blastemal cells (Figure 5*B*) and very intense nuclear and cytoplasmic staining was observed in the tumor stroma (Figure 5*C*) in 11 of the 13 tumors. No iNOS expression was observed in two tumors. Overall, iNOS expression was significantly higher in tumors than in control kidneys (Figure 5*D*).

Nitrotyrosine. NT expression was very low in control kidneys (Figure 5*E*). In all 13 tumors analyzed, the blastemal components displayed diffuse cytoplasmic staining for NT (Figure 5*F*), whereas stromal components displayed both nuclear and cytoplasmic staining for this marker (Figure 5*G*). NT expression in tumors was significantly higher than in control kidneys (Figure 5*H*).

Vascular endothelial growth factor. In normal kidneys, VEGF expression was observed in proximal and distal convoluted tubules (Figure 5*I*). VEGF expression was observed in the stroma of all 13 tumor specimens analyzed (Figure 5*K*). It also was observed, but to a lesser degree, in blastemal (Figure 5*J*) and epithelial (data not shown) components of the tumors. This pattern of VEGF expression was similar to those of COX-2 (Figure 4*C*) and HIF-1 (Figure 4*G*). The VEGF expression in tumors was significantly higher than that in control kidney sections (Figure 5*L*). Expression of various inflammatory markers in different parts of the tumor was summarized in Table W3. Though tumors used in the current study were different stages of WT disease, we did not notice any difference in the infiltration of inflammatory cells and expression pattern of different inflammatory markers.

Characterization of Inflammation in Mouse Tumors

The characterization of inflammatory marker studies was extended to the mouse model of WT to confirm their expression. Similar to human tumors, very robust expression of COX-2 was observed in mouse tumors (Figure 6*B*) compared to mouse control kidneys (Figure 6*A*). Similarly, increased TAM (F4/80) infiltration was observed in mouse tumors (Figure 6*D*) compared to control kidneys (Figure 6*C*).

Expression Pattern of Inflammatory Markers in the Tumor Stroma Similar to that of TAM Recruitment

The expression of the inflammatory markers COX-2, HIF-1, iNOS, p-ERK1/2, and VEGF was predominantly localized to tumor stroma, similar to the localization of TAMs (Figures 1–5 and W1). The co-distribution of major inflammatory marker COX-2 with TAM infiltration in the tumor stroma was analyzed by double immunofluorescence analysis (Figure 7). The COX-2 expression (Figure 7, *B* and *D*) and TAM infiltration (Figure 7, *C* and *D*) was almost undetectable in control kidney samples (Figure 7, *A*–*D*), but there was very prominent expression of COX-2 (Figure 7, *F* and *H*) and very huge infiltration of TAMs (Figure 7, *G* and *H*) in the tumor stroma was noticed. This suggests that infiltration of inflammatory immune cells and the expression of inflammatory markers in the tumor stroma are related.

Discussion

While it has been previously established that an inflammatory microenvironment plays a significant role in the establishment and progression of adult-onset cancers, the potential contribution of the inflammatory microenvironment in childhood cancers has not yet been adequately addressed. We have investigated the role of the inflammatory microenvironment in a panel of 14 WTs, a pediatric cancer of the kidney. Our qualitative and quantitative IHC assessment of immune cells and inflammatory protein markers in WT revealed infiltration of both adaptive and innate immune cells. The extent of infiltration varied among tumors and also among histologically distinct regions within the same tumor. Interestingly, adaptive immune cells (T and B cells) were localized predominantly to the tumor stroma. In contrast, innate immune cells (TAMs, TINs, and MCs), while localized predominantly in the tumor stroma, were also present in all other regions of the tumor.

In our panel of WTs, we also observed increased expression of inflammatory proteins such as VEGF, HIF-1, and COX-2, which have previously been noted to be elevated in WT [5,7,8], and iNOS and NT, which had not been noted before in these tumors. The majority of these inflammatory proteins were, like the immune cells, primarily localized to the tumor stroma. This observation suggests a correlation between the infiltrating immune cells and the activated cytokines and chemokines. The co-localization of the inflammatory proteins and the TAMs was especially striking, as TAM was the predominant type of infiltrating immune cell in WTs in the present study. This TAM infiltration was further confirmed (F4/80 expression) in the mouse model of WT. TAM infiltration is known to be induced by COX-2 in the tumor microenvironment [10], especially in the tumor stroma, and TAMs can also induce expression of COX-2 [11]. Our double immunofluorescence analysis of COX-2 and TAMs in the tumor stroma supports the co-distribution of these inflammatory markers and suggests that these inflammatory markers may activate each other in the tumor microenvironment.

Studies have shown that TAMs are also involved in the production of proangiogenic factors transforming growth factor β and VEGF [12,13] and of immunosuppressive chemokines and cytokines such as interleukin 10 and prostaglandin E_2, which contribute to tumor angiogenesis [12,14–16]. Thus, the TAM infiltration we observed in our panel of WTs may play a significant role in the increased VEGF expression also seen in these tumors and hence also in the vascularization of the tumors.

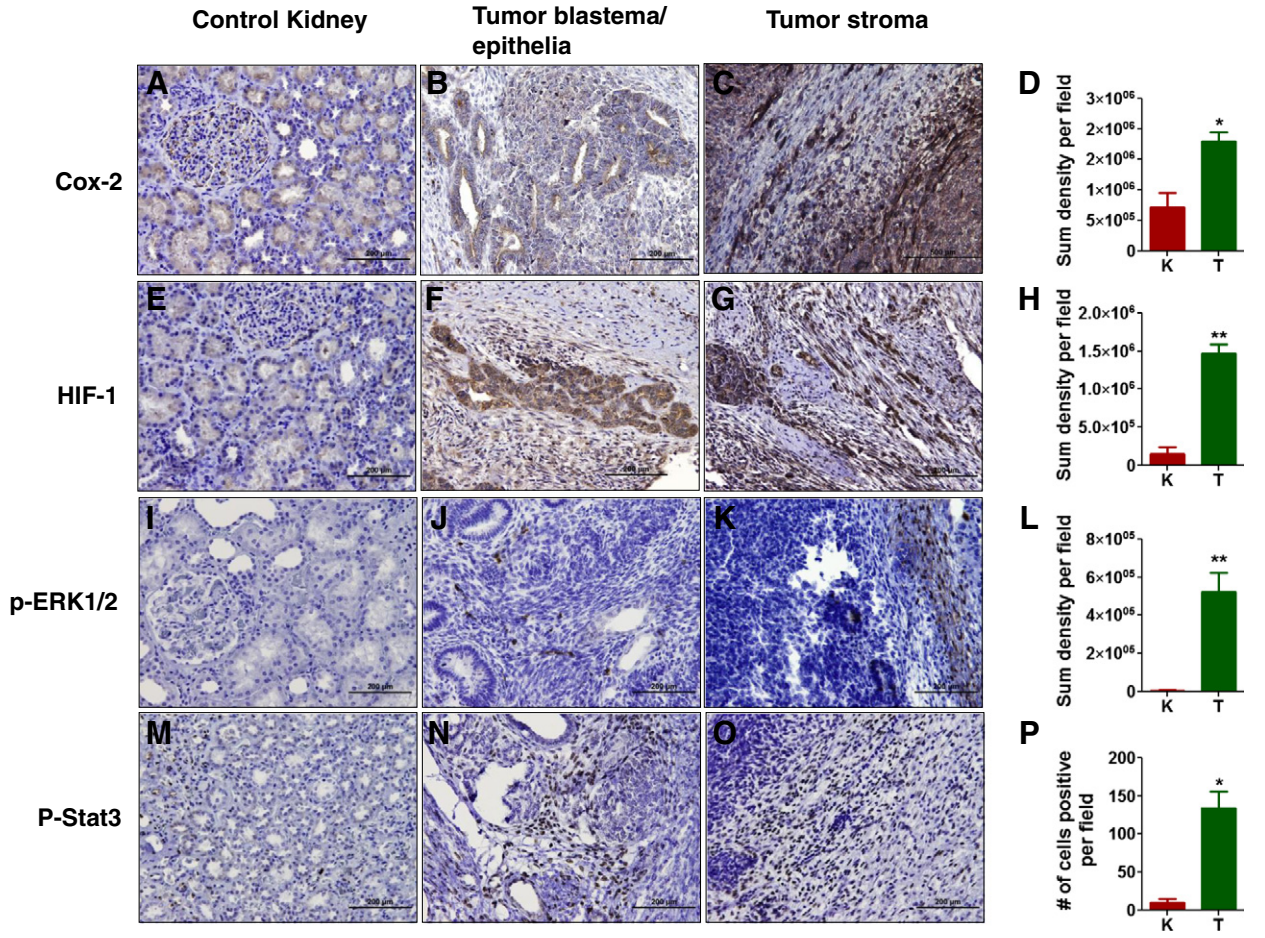

Figure 4. Overexpression of inflammatory markers in WTs. (A–C) Representative COX-2 expression in (A) normal kidneys, (B) tumor blastema/epithelia, and (C) tumor stroma. (D) Quantification of sum density of COX-2 expression per field in normal kidneys (K) and tumors (T). (E–G) Representative HIF-1 expression in (E) normal kidneys, (F) tumor blastema/epithelia, and (G) tumor stroma. (H) Sum density of HIF-1 per field in normal kidneys and tumors. (I–K) Representative p-ERK1/2 expression in (I) normal kidneys, (J) tumor blastema/epithelia, and (K) tumor stroma. (L) Sum density of p-ERK1/2 expression per field in normal kidneys and tumors. (M–O) Representative p-Stat3 expression in (M) normal kidneys, (N) tumor blastema/epithelia, and (O) tumor stroma. (P) Sum density of p-Stat3 expression per field in normal kidneys and tumors. Negative controls expressed none of these markers. $^{*}P \leq .05$, $^{**}P \leq .01$.

A previous study examined infiltration of tumor-associated leukocytes in a small group of five WTs and noted the presence of T cells and macrophages in these tumors [6]. We have verified the presence of these immune cells in our larger panel of tumors and have expanded this analysis to include B cells, TINs, and MCs as well as inflammatory markers and have established the localization of these immune cell types and inflammatory markers within the tumors.

As already noted, our study is unique in the demonstration of expression of iNOS and NT in the tumor stroma in WTs. Increased expression of iNOS and COX-2 has been reported in various other tumors [17], and other studies have demonstrated a correlation between the expression of iNOS and NT and that of COX-2 [18] and their spatial co-localization with TAM infiltration and VEGF expression [19,20]. Our data suggest a role for TAMs and COX-2 expression in the up-regulation of expression of iNOS and NT in the tumor stroma. Furthermore, the abundant expression of COX-2 along with iNOS and NT in the tumor stroma may have induced HIF-1 expression in the tumors, and this, in turn, may also upregulate the expression of VEGF.

One of the predominant inflammatory protein markers overexpressed in all of our WTs was COX-2, which was highly expressed in the tumor stroma and, to a lesser degree, in all other tumor components. The COX-2 expression was further confirmed in the mouse model of WT, which has shown a similar expression pattern with the human tumors. This spatial expression is in marked contrast to the findings of previous studies that reported moderate to strong cytoplasmic expression of COX-2 in blastemal and epithelial components of the tumors but no expression in the tumor stroma [8].

Various mechanisms could be responsible, individually or in combination, for the abundant COX-2 expression in WTs. First, the infiltrating immune cells themselves could be overexpressing COX-2. Second, tumor fibroblasts could be generating COX-2 in response to macrophage infiltration or the inflammatory tumor microenvironment. Third, COX-2 expression in these tumors may be induced by fetal mitogen IGF2 through the Ras/Raf/Mitogen-activated protein kinase kinase also known as MEK/ERK pathway, as has been reported in human keratinocytes [21]. Overexpression of IGF2 has been reported in various cancers [22–25], including 70% of WTs [26,27]. We have previously reported upregulated p-ERK1/2 expression in mouse WTs engineered to overexpress IGF2 and also in human WTs [9], suggesting a role for ERK signaling in WT development. The robust expression of COX-2 and p-ERK1/2 we observed in the current series of tumors further suggests that one consequence of

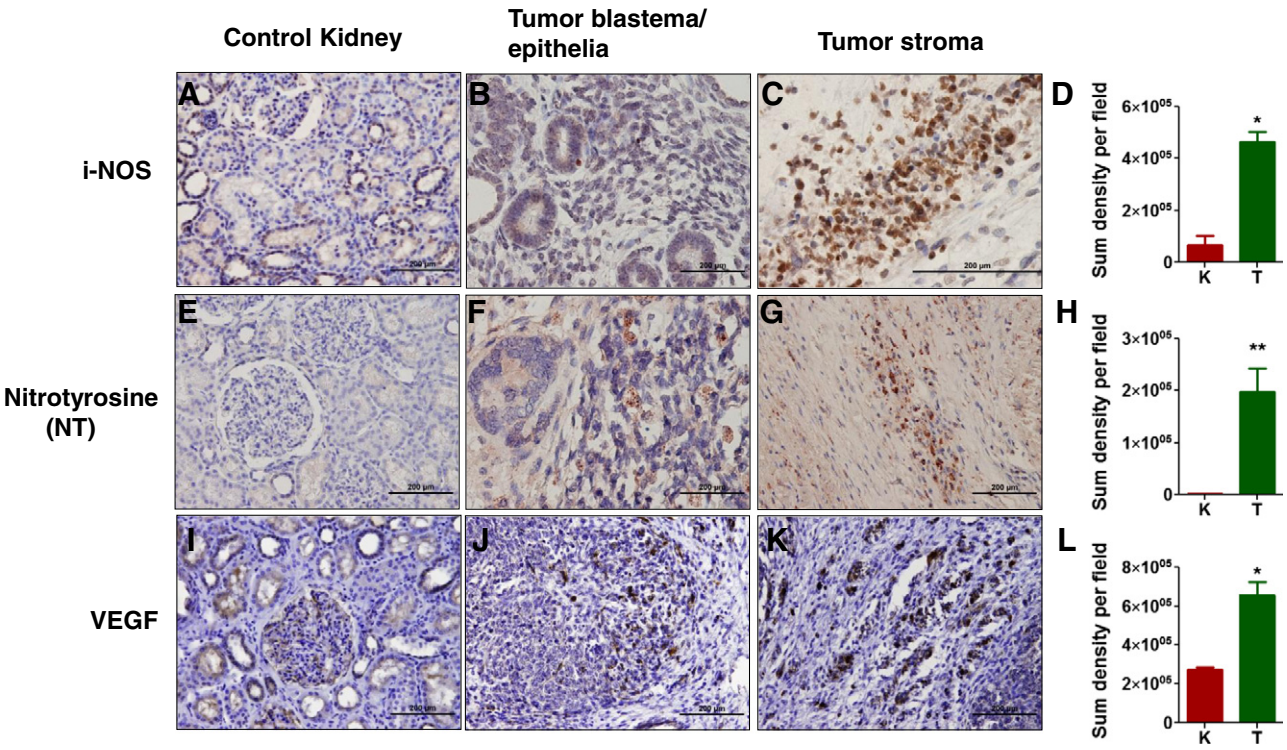

Figure 5. TAM-induced expression of inflammatory markers in WTs. (A–C) Representative iNOS expression in (A) normal kidneys, (B) tumor blastema/epithelia, and (C) tumor stroma. (D) Quantification of sum density of iNOS expression per field in normal kidneys (K) and tumors (T). (E–G) Representative NT expression in (E) normal kidneys, (F) tumor blastema/epithelia, and (G) tumor stroma. (H) Sum density of NT expression per field in normal kidneys and tumors. (I–K) Representative VEGF expression per field in (I) normal kidneys, (J) tumor blastema/epithelia, and (K) tumor stroma. (L) Sum density of VEGF expression per field in normal kidneys and tumors. *$P \leq .05$, **$P \leq .01$.

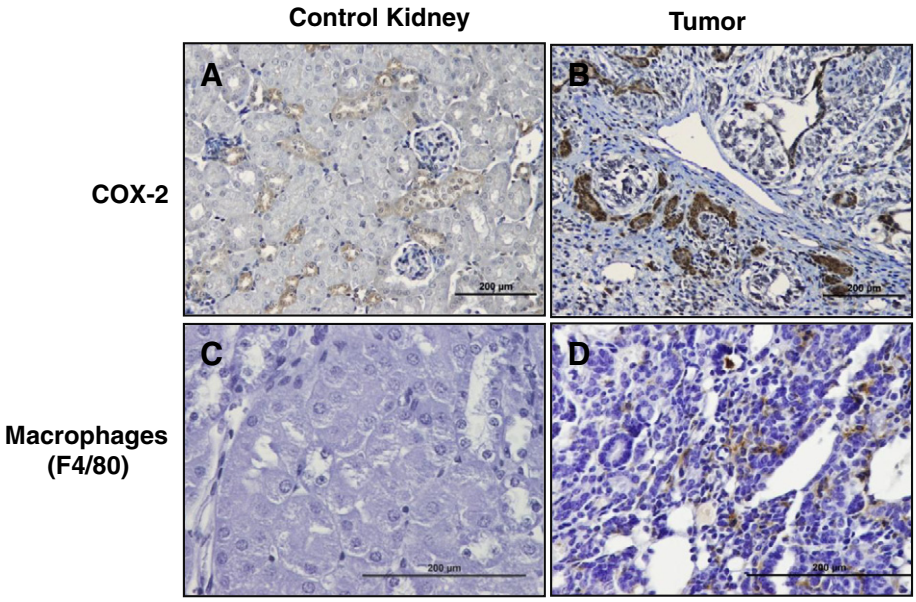

Figure 6. Overexpression of major inflammatory marker COX-2 and infiltration of predominant inflammatory immune cells, TAMs (F4/80+ve macrophages), in the mouse model of WT (A–D). Representative COX-2 expression (×200) in (A) normal mouse kidney and (B) mouse tumor. (C and D) Representative TAM infiltration (×400) in (C) normal kidney and (D) mouse tumor.

IGF2 over expression in WTs is COX-2 up-regulation and promotion of an inflammatory microenvironment and that this effect is mediated by enhanced p-ERK signaling.

COX-2 can also activate the expression of HIF-1 through its enzymatic product prostaglandin E_2 [21,28]. The expression of COX-2 and HIF-1 was spatially similar in the tumors we assessed.

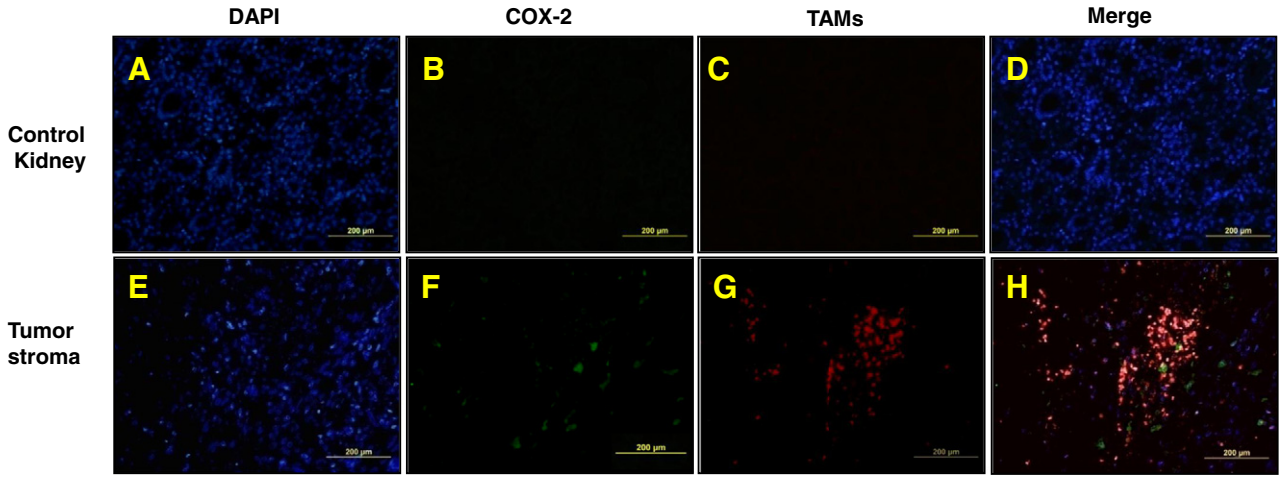

Figure 7. Expression pattern of major inflammatory marker COX-2 with TAM infiltration in the tumor stroma. To characterize the similar localization of these two markers in the tumor stroma, double immunofluorescence staining was performed (A–H). Though in the control kidneys staining for COX-2 (B and D) and TAMs (C and D) was not observed (A–D), in the tumor stroma, COX-2 (F and H) expression was observed where predominant infiltrating immune cells, TAMs (G and H), were infiltrated (E–H).

HIF-1 expression was predominantly nuclear in the tumor stroma, with granular cytoplasmic and membranous expression in blastemal and epithelial regions, which is consistent with a previous report [5]. COX-2 activation of HIF-1 can also occur through hypoxia [5] or hypoxia-independent mechanisms [29], the latter involving p-ERK1/2 [30]. As already noted, we observed expression of p-ERK1/2 in a majority of tumors in the present study and also in our mouse model of WT [9]. HIF-1 can also directly upregulate expression of COX-2 during hypoxia [31] and thus form a feedback loop to continually activate the COX-2 pathway. Hence, we speculate that COX-2 in this WT microenvironment may drive the inflammation and upregulate the aforementioned downstream targets.

Thus, the current work represents a qualitative, quantitative, and spatial assessment of various inflammatory immune cells and inflammatory protein markers in WT. The correlation and localization of TAMs in the tumor stroma with expression of various inflammatory protein markers, such as COX-2, HIF-1, p-ERK1/2, iNOS, and NT, suggest a functional association of TAM infiltration with the overexpression of these markers (our double immunofluorescence data confirmed the same) and *vice versa* in WTs and demonstrate the existence of a highly inflammatory microenvironment in this disease. Overexpression of inflammatory markers in tumors, in particular COX-2, has provided a rationale for their targeting in prevention and treatment of many cancers [32–36], by COX-2–specific inhibitors alone [37–39] or in combination with other inhibitors [40,41]. The current work suggests that such an approach may also be of utility for WTs.

Supplementary data to this article can be found online at http://dx.doi.org/10.1016/j.neo.2014.05.008.

References

[1] Mantovani A, Allavena P, Sica A, and Balkwill F (2008). Cancer-related inflammation. *Nature* **454**, 436–444.
[2] Grivennikov SI, Greten FR, and Karin M (2010). Immunity, inflammation, and cancer. *Cell* **140**, 883–899.
[3] Colotta F, Allavena P, Sica A, Garlanda C, and Mantovani A (2009). Cancer-related inflammation, the seventh hallmark of cancer: links to genetic instability. *Carcinogenesis* **30**, 1073–1081.
[4] Mantovani A (2009). Cancer: inflaming metastasis. *Nature* **457**, 36–37.
[5] Karth J, Ferrer FA, Perlman E, Hanrahan C, Simons JW, Gearhart JP, and Rodriguez R (2000). Coexpression of hypoxia-inducible factor 1-alpha and vascular endothelial growth factor in Wilms' tumor. *J Pediatr Surg* **35**, 1749–1753.
[6] Vakkila J, Jaffe R, Michelow M, and Lotze MT (2006). Pediatric cancers are infiltrated predominantly by macrophages and contain a paucity of dendritic cells: a major nosologic difference with adult tumors. *Clin Cancer Res* **12**, 2049–2054.
[7] Giordano G, Campanini N, Donofrio V, Bertolini P, Falleti J, Grassani C, and Pettinato G (2008). Analysis of Cox-2 expression in Wilms' tumor. *Pathol Res Pract* **204**, 875–882.
[8] Fridman E, Pinthus JH, Kopolovic J, Ramon J, Mor O, and Mor Y (2006). Expression of cyclooxygenase-2 in Wilms tumor: immunohistochemical study using tissue microarray methodology. *J Urol* **176**, 1747–1750.
[9] Hu Q, Gao F, Tian W, Ruteshouser EC, Wang Y, Lazar A, Stewart J, Strong LC, Behringer RR, and Huff V (2011). *Wt1* ablation and *Igf2* upregulation in mice result in Wilms tumors with elevated ERK1/2 phosphorylation. *J Clin Invest* **121**, 174–183.
[10] Tjiu JW, Chen JS, Shun CT, Lin SJ, Liao YH, Chu CY, Tsai TF, Chiu HC, Dai YS, and Inoue H, et al (2009). Tumor-associated macrophage-induced invasion and angiogenesis of human basal cell carcinoma cells by cyclooxygenase-2 induction. *J Invest Dermatol* **129**, 1016–1025.
[11] Hou Z, Falcone DJ, Subbaramaiah K, and Dannenberg AJ (2011). Macrophages induce COX-2 expression in breast cancer cells: role of IL-1β autoamplification. *Carcinogenesis* **32**, 695–702.
[12] Mantovani A, Sozzani S, Locati M, Allavena P, and Sica A (2002). Macrophage polarization: tumor-associated macrophages as a paradigm for polarized M2 mononuclear phagocytes. *Trends Immunol* **23**, 549–555.
[13] Bingle L, Brown NJ, and Lewis CE (2002). The role of tumour-associated macrophages in tumour progression: implications for new anticancer therapies. *J Pathol* **196**, 254–265.
[14] Balkwill F, Charles KA, and Mantovani A (2005). Smoldering and polarized inflammation in the initiation and promotion of malignant disease. *Cancer Cell* **7**, 211–217.
[15] Pollard JW (2004). Tumour-educated macrophages promote tumour progression and metastasis. *Nat Rev Cancer* **4**, 71–78.
[16] Van Ginderachter JA, Movahedi K, Hassanzadeh Ghassabeh G, Meerschaut S, Beschin A, Raes G, and De Baetselier P (2006). Classical and alternative activation of mononuclear phagocytes: picking the best of both worlds for tumor promotion. *Immunobiology* **211**, 487–501.
[17] Rahman MA, Dhar DK, Yamaguchi E, Maruyama S, Sato T, Hayashi H, Ono T, Yamanoi A, Kohno H, and Nagasue N (2001). Coexpression of inducible nitric oxide synthase and COX-2 in hepatocellular carcinoma and surrounding liver: possible involvement of COX-2 in the angiogenesis of hepatitis C virus-positive cases. *Clin Cancer Res* **7**, 1325–1332.
[18] Klimp AH, Hollema H, Kempinga C, van der Zee AG, de Vries EG, and Daemen T (2001). Expression of cyclooxygenase-2 and inducible nitric oxide

synthase in human ovarian tumors and tumor-associated macrophages. *Cancer Res* **61**, 7305–7309.
[19] Feng CW, Wang LD, Jiao LH, Liu B, Zheng S, and Xie XJ (2002). Expression of p53, inducible nitric oxide synthase and vascular endothelial growth factor in gastric precancerous and cancerous lesions: correlation with clinical features. *BMC Cancer* **2**, 2–8.
[20] Sikora AG, Gelbard A, Davies MA, Sano D, Ekmekcioglu S, Kwon J, Hailemichael Y, Jayaraman P, Myers JN, and Grimm EA, et al (2010). Targeted inhibition of inducible nitric oxide synthase inhibits growth of human melanoma in vivo and synergizes with chemotherapy. *Clin Cancer Res* **16**, 1834–1844.
[21] Kim HJ and Kim TY (2004). IGF-II-mediated COX-2 gene expression in human keratinocytes through extracellular signal-regulated kinase pathway. *J Invest Dermatol* **123**, 547–555.
[22] Cui H, Cruz-Correa M, Giardiello FM, Hutcheon DF, Kafonek DR, Brandenburg S, Wu Y, He X, Powe NR, and Feinberg AP (2003). Loss of IGF2 imprinting: a potential marker of colorectal cancer risk. *Science* **299**, 1753–1755.
[23] Osborne CK, Coronado EB, Kitten LJ, Arteaga CI, Fuqua SA, Ramasharma K, Marshall M, and Li CH (1989). Insulin-like growth factor-II (IGF-II): a potential autocrine/paracrine growth factor for human breast cancer acting via the IGF-I receptor. *Mol Endocrinol* **3**, 1701–1709.
[24] D'Errico A, Grigioni WF, Fiorentino M, Baccarini P, Lamas E, De Mitri S, Gozzetti G, Mancini AM, and Brechot C (1994). Expression of insulin-like growth factor II (IGF-II) in human hepatocellular carcinomas: an immunohistochemical study. *Pathol Int* **44**, 131–137.
[25] Tennant MK, Thrasher JB, Twomey PA, Birnbaum RS, and Plymate SR (1996). Insulin-like growth factor-binding proteins (IGFBP)-4, -5, and -6 in the benign and malignant human prostate: IGFBP-5 messenger ribonucleic acid localization differs from IGFBP-5 protein localization. *J Clin Endocrinol Metab* **81**, 3783–3792.
[26] Sparago A, Cerrato F, Vernucci M, Ferrero GB, Silengo MC, and Riccio A (2004). Microdeletions in the human H19 DMR result in loss of IGF2 imprinting and Beckwith-Wiedemann syndrome. *Nat Genet* **36**, 958–960.
[27] Prawitt D, Enklaar T, Gartner-Rupprecht B, Spangenberg C, Lausch E, Reutzel D, Fees S, Korzon M, Brozek I, and Limon J, et al (2005). Microdeletion and IGF2 loss of imprinting in a cascade causing Beckwith-Wiedemann syndrome with Wilms' tumor. *Nat Genet* **37**, 785–786 [author reply 786-787].
[28] Kirkpatrick K, Ogunkolade W, Elkak A, Bustin S, Jenkins P, Ghilchik M, and Mokbel K (2002). The mRNA expression of cyclo-oxygenase-2 (COX-2) and vascular endothelial growth factor (VEGF) in human breast cancer. *Curr Med Res Opin* **18**, 237–241.
[29] Zhong H, Agani F, Baccala AA, Laughner E, Rioseco-Camacho N, Isaacs WB, Simons JW, and Semenza GL (1998). Increased expression of hypoxia inducible factor-1α in rat and human prostate cancer. *Cancer Res* **58**, 5280–5284.
[30] Bilton RL and Booker GW (2003). The subtle side to hypoxia inducible factor (HIFα) regulation. *Eur J Biochem* **270**, 791–798.
[31] Greenhough A, Smartt HJ, Moore AE, Roberts HR, Williams AC, Paraskeva C, and Kaidi A (2009). The COX-2/PGE2 pathway: key roles in the hallmarks of cancer and adaptation to the tumour microenvironment. *Carcinogenesis* **30**, 377–386.
[32] Rahman M, Selvarajan K, Hasan MR, Chan AP, Jin C, Kim J, Chan SK, Le ND, Kim YB, and Tai IT (2012). Inhibition of COX-2 in colon cancer modulates tumor growth and MDR-1 expression to enhance tumor regression in therapy-refractory cancers in vivo. *Neoplasia* **14**, 624–633.
[33] Sarkar FH, Adsule S, Li Y, and Padhye S (2007). Back to the future: COX-2 inhibitors for chemoprevention and cancer therapy. *Mini Rev Med Chem* **7**, 599–608.
[34] Arun B and Goss P (2004). The role of COX-2 inhibition in breast cancer treatment and prevention. *Semin Oncol* **31**, 22–29.
[35] Brandão RD, Veeck J, Van de Vijver KK, Lindsey P, de Vries B, van Elssen CH, Blok MJ, Keymeulen K, Ayoubi T, and Smeets HJ, et al (2013). A randomised controlled phase II trial of pre-operative celecoxib treatment reveals anti-tumour transcriptional response in primary breast cancer. *Breast Cancer Res* **15**, R29.
[36] Yang YH, Cheng CL, Ho PS, and Ko YC (2012). The role of chemoprevention by selective cyclooxygenase-2 inhibitors in colorectal cancer patients – a population-based study. *BMC Cancer* **12**, 582.
[37] Bae SH, Jung ES, Park YM, Kim BS, Kim BK, Kim DG, and Ryu WS (2001). Expression of cyclooxygenase-2 (COX-2) in hepatocellular carcinoma and growth inhibition of hepatoma cell lines by a COX-2 inhibitor, NS-398. *Clin Cancer Res* **7**, 1410–1418.
[38] Parashar B, Latha Shankar S, O'Guin K, Butler J, Vikram B, and Shafit-Zagardo B (2005). Inhibition of human neuroblastoma cell growth by CAY10404, a highly selective Cox-2 inhibitor. *J Neurooncol* **71**, 141–148.
[39] Zhao Q, Wang C, Zhu J, Wang L, Dong S, Zhang G, and Tian J (2011). RNAi-mediated knockdown of cyclooxygenase2 inhibits the growth, invasion and migration of SaOS2 human osteosarcoma cells: a case control study. *J Exp Clin Cancer Res* **30**, 26.
[40] Dickens DS and Cripe TP (2003). Effect of combined cyclooxygenase-2 and matrix metalloproteinase inhibition on human sarcoma xenografts. *J Pediatr Hematol Oncol* **25**, 709–714.
[41] Zhang LJ, Wang SY, Huo XH, Zhu ZL, Chu JK, Ma JC, Cui DS, Gu P, Zhao ZR, and Wang MW, et al (2009). Anti-*Helicobacter pylori* therapy followed by celecoxib on progression of gastric precancerous lesions. *World J Gastroenterol* **15**, 2731–2738.